applied sciences

MDPI

Article

Seismic Benefits from Coupling Frame Structures with a Hysteretic Mass Damper Inerter

Angelo Di Egidio [1,†] and Alessandro Contento [2,*,†]

[1] Department of Civil, Construction-Architectural and Environmental Engineering, University of L'Aquila, 67100 L'Aquila, Italy
[2] College of Engineering, Fuzhou University, Fuzhou 350025, China
* Correspondence: alessandro@fzu.edu.cn
† These authors contributed equally to this work.

Abstract: The coupling of frame structures with external oscillating bodies, such as rigid walls, dynamic mass absorbers, elastoplastic dampers, or tuned mass dampers, can be effective in reducing the displacements of the structure and protecting it against seismic loads. This paper proposes connecting an external oscillating body to the first story of a frame structure and studying the effectiveness of the coupling by evaluating the reduction in the displacements of the frame structure. The inertial effects of the oscillating body are increased by introducing a virtual mass, provided by an inerter device. The oscillating body, characterized by physical and virtual masses, is connected to the frame structure through a hysteretic device. The study is performed on a dynamically equivalent three-degree-of-freedom (3-DOF) model, whose equations are written using a direct approach. To verify the effectiveness of the protection device, named hysteretic mass damper inerter (HMDI), in reducing the displacements of the frame structure, the displacement of the first story and the drifts of the upper stories are compared to those of the frame structure not connected to the external oscillating body. An initial spectral analysis, performed on the linearized mechanical system, clarifies the role of the parameters of the external device in the dynamic behavior of the coupled system. An additional seismic analysis is performed by using three single earthquake records first, and then a set of seven additional earthquake records selected to be compatible with the design spectrum of Los Angeles. Specific spectral gain maps are used to organize the results of an extensive parametric analysis. They show that the HMDI reduces both displacements and drifts of the structure in large ranges of the parameters that characterize the HMDI. It is found that the proposed protection method is particularly effective for low- and medium-rise frame structures.

Keywords: frame structure; hysteretic mass damper; inerter device; dynamic and seismic performance

check for updates

Citation: Di Egidio, A.; Contento, A. Seismic Benefits from Coupling Frame Structures with a Hysteretic Mass Damper Inerter. *Appl. Sci.* **2023**, *13*, 5017. https://doi.org/10.3390/app13085017

Academic Editor: Andrea Carpinteri

Received: 1 March 2023
Revised: 10 April 2023
Accepted: 11 April 2023
Published: 17 April 2023

Copyright: © 2023 by the authors. Licensee MDPI, Basel, Switzerland. This article is an open access article distributed under the terms and conditions of the Creative Commons Attribution (CC BY) license (https://creativecommons.org/licenses/by/4.0/).

1. Introduction

The protection of new and existing structures against seismic actions is a fundamental topic in civil engineering and has been widely studied. The seismic protection of a structure can be achieved at two different stages: either from the beginning, during the design process, or through retrofitting, for existing structures. Different approaches are used to study the protection of structures. Depending on the interests and the stage of development of the protection techniques, some studies use low-dimensional mechanical models to investigate the suitability of the typology of a device for the protection of structures, while other studies use sophisticated models primarily by performing numerical simulations with finite element models to evaluate the efficiency of a protection technique based on devices with specific characteristics.

This paper belongs to the first category, and a low-dimensional mechanical model (i.e., an archetype model) is used to describe the main seismic behavior of structures with and without the connection to a prospective protection device. Several papers available in the

literature propose similar approaches based on low-dimensional models. For example, 2-DOF models were used to study the advantages of base isolation in [1] and the effectiveness of the protection through tuned mass dampers (TMD) in [2–4]. Similarly, in [5,6], 2-DOF models were used to investigate the ability of a TMD to reduce the base displacement of a base-isolated system. Moreover, in [7,8], the behavior of a structure placed on a rocking podium is investigated using low-dimensional models. Additionally, in [9–12], archetype models were used to analyze the seismic performances of coupling a frame structure with an external rocking wall. More recently, the effectiveness of coupling a frame structure with external systems equipped with inerter devices and a yielding exoskeleton was studied in [13,14], respectively. Low-dimensional models were also used to describe the dynamics of rigid body-like structures, as in [15,16], where different active control algorithms were considered to improve the seismic performance of such structures. The seismic effectiveness of an intermediate discontinuity in a frame structure was studied in [17,18] by using a 2-DOF mechanical model; in [19,20], the authors performed analytical and experimental investigations on frame structures with inter-story isolation by using a 3-DOF model.

The idea behind the protection device studied in this paper is derived from studies of protection systems based on TMDs connected with structures to protect by viscoelastic devices. To ensure the effectiveness of a TMD, a small mass is usually sufficient. However, in the case of seismic excitation, the use of a small mass may undermine the effectiveness of the TMD. This issue can be addressed by coupling the TMD with an inerter device that increases its inertial forces, as described in [21]. Inerter devices and their applications, mostly related to the control of engineering structures, have been studied for about two decades and, at the state-of-the-art, several types of inerter devices and relative models have been proposed [22] and experimentally tested [23–25]. Some studies fully characterized the nonlinear behavior of the inerter device that may play a significant role in some applications, such as the one proposed in this paper. The device obtained by coupling a TMD with an inerter device, named tuned mass damper inerter (TMDI), was investigated in several papers [26–31], some of which specifically focused on increasing the efficiency of base isolation [32]. Moreover, in the case of TMDIs, several studies were carried out on archetype or simplified models with a limited number of DOFs [33].

Following a similar approach, this paper investigates the possible improvement of the dynamic behavior of a frame structure by coupling it with an external oscillating body linked to the first story of the frame structure through a hysteretic coupling device. Moreover, in this case, the inertial effects of the oscillating body are increased by using an inerter device. Such a protection device, which comprises the oscillating body, the connection device, and the inerter device, is called a hysteretic mass damper inerter (HMDI), similar to the TMDI, and has already been used in [34] for the protection of rigid block-like structures against seismic excitation. The purpose of this study is to understand if the HMDI can reduce the displacement of the first story and the drifts of the upper stories without modifying the properties of the frame structure to protect. The coupled structure (i.e., the structure plus the protection device) is modeled by a 3-DOF analytical model described by equations of motion written using a direct approach. The behavior of the hysteretic coupling device is modeled by the classic Bouc–Wen constitutive law [35].

A preliminary spectral analysis is performed on the linearized mechanical system to investigate the dynamics of the coupled system. The evaluation of the modal mass participating coefficient (MPC) of the oscillating modes allows for investigating the importance of the oscillating modes of the coupled system. After the preliminary spectral analysis, a seismic analysis is conducted by using three single earthquake records first, and then a set of seven additional earthquake records selected to be compatible with the design spectrum of Los Angeles. The effectiveness of the HMDI in protecting the frame structure is quantified by defining two gain coefficients. The first provides the ratio between the displacements of the first story of the structure connected (or not) to the HMDI. Similarly, the second provides the ratio between the drifts of the upper stories of the structure in the

two cases. The results are arranged in spectral gain maps that represent the contour plots of the gain coefficients in a specific parameter plane.

After the introduction, the second section presents the mechanical models of both the frame structure equipped with the protection device and the reference frame structure. The third section discusses the parameters that are varied in the spectral and seismic analyses presented in the fourth and fifth sections, respectively. Both analyses compare the behavior of the frame structure with and without the HMDI. In particular, the fifth section, which is devoted to seismic analyses, includes both analyses performed with a single earthquake record and analyses performed with a set of spectrum-compatible earthquake records. The findings of the research are summarized in the conclusions section.

2. Mechanical Model

The multi-degree-of-freedom (M-DOF) mechanical model presented in this section describes the behavior of a multi-DOF frame structure coupled with the protection device. As already mentioned, the device, named a hysteretic mass damper inerter (HMDI), is composed of an oscillating mass and an inerter device used to increase its inertial force. The HMDI is linked to the first story of the frame structure by a hysteretic connection (see Figure 1). As shown in Figure 1, from an aesthetic point of view, the HMDI can be particularly effective if it can be connected to the underground level (if it is present), by placing the HMDI just below the entrance level (i.e., street level) of the building.

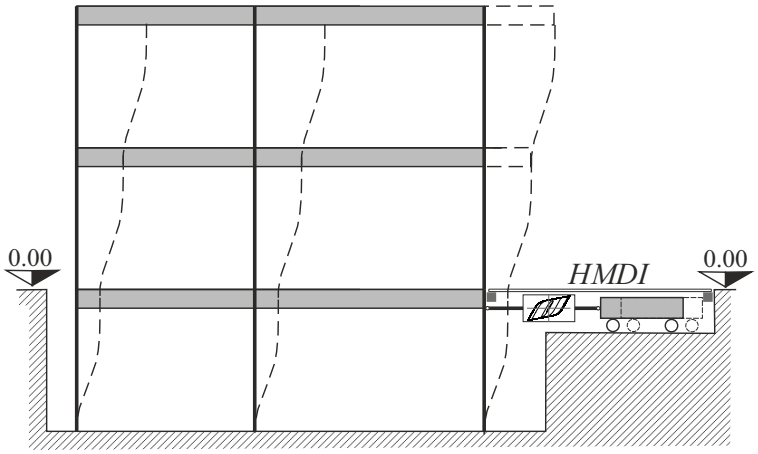


Figure 1. Frame structure coupled with the HMDI at the first story.

2.1. Equations of Motion

Figure 2 shows the simplified structure, which is the reference for the low-dimensional mechanical model used to capture the behavior of the multi-DOF frame structure linked to the HMDI. Specifically, a 2-DOF shear-type structural model is used to describe the main dynamics of the frame structure, regardless of the number of its stories. The mechanical characteristics of such a 2-DOF model are obtained by using the dynamic equivalence criterion defined in [18], which was developed mainly for low- and medium-rise frame structures. The dynamical equivalence consists in determining both the equivalent stiffness coefficients k_1 and k_2, and the masses m_1 and m_2 that correspond to the masses of the first story and the sum of the masses of all the stories above the first one, respectively (Figure 2a). According to the procedure presented in [18], to derive the values for the equivalent characteristics, the DOFs u_1 and u_2 have to correspond to the displacements of the first and top stories of the structure, respectively. The following additional assumptions are at the base of the equivalence criterion:

- The circular frequencies ω of the leading mode of the M-DOF frame structure and of the first mode of the 2-DOF system (Figure 2) are the same;
- The modal components of the first and top stories of the frame structure are equal to the modal components u_1 and u_2 of the equivalent low-dimensional system.

Furthermore, the Rayleigh formulation is used to derive the damping coefficients of the equivalent 2-DOF model by considering the damping ratio $\xi = 0.05$ for both modes.

A simple 1-DOF system with displacement u_{ext} (Figure 2b) describes the HMDI. The physical mass m of the external oscillating system is increased through an inerter device with inertance (or virtual mass) m_I and is linked to the first story of the frame structure through a hysteretic connection described by the classical Bouc–Wen model [35]. The equations of motion of the 3-DOF system composed of the 2-DOF share-type structural model plus the protection device are obtained with a direct approach, such as,

$$\begin{aligned} &m_1\ddot{u}_1(t) + c_1\dot{u}_1(t) - c_{12}\dot{u}_2(t) + (k_1 + k_2)u_1(t) - k_2u_2(t) - F_H = -m_1\ddot{x}_g(t), \\ &m_2\ddot{u}_2(t) - c_{12}\dot{u}_1(t) + c_2\dot{u}_2(t) - k_2u_1(t) + k_2u_2(t) = -m_2\ddot{x}_g(t), \\ &(m + m_I)\ddot{u}_{ext}(t) + F_H = -m\ddot{u}_g(t), \end{aligned} \tag{1}$$

where the external excitation is denoted by $\ddot{u}_g$, and F_H is the coupling hysteretic force. The three equations (Equation (1)) represent the equilibrium of the forces acting on the masses m_1, m_2, and $m + m_I$, respectively. Moreover, Equation (1) (third line equation) shows that the external excitation $\ddot{u}_g$ acts only on the physical mass m of the protection device, whereas the virtual mass m_I is only affected by the relative acceleration $\ddot{u}_{ext}$ acting on its connection points. The application of the Rayleigh method provides a full symmetric damping matrix $\mathbf{C} = \alpha\mathbf{M} + \beta\mathbf{K}$, where quantities $c_{12} = c_{21}$, in Equation (1), are the off-diagonal terms of $\mathbf{C}$.

According to the Bouc–Wen model [35], the restoring hysteretic force F_H can be expressed as

$$F_H = \psi k_c(u_{ext}(t) - u_1(t)) + k_c u_y(1 - \psi)z(t). \tag{2}$$

In Equation (2), the ratio between post-yielding stiffness k_{plast} and pre-yielding stiffness is represented by ψ (i.e., $k_{\text{plast}} = \psi k_c$). The case with $\psi = 0$ describes the elastic perfectly plastic behavior of the connection device; $\psi = 1$ represents a fully elastic behavior. The yielding force of the hysteretic connection F_y is provided by the product $k_c u_y$, with u_y being the yielding displacement. Finally, $z(t)$ is a hysteretic variable that describes the post-yielding behavior and is evaluated by solving the following nonlinear first-order ordinary differential equation

$$\dot{z}(t) = \frac{\dot{u}_{ext}(t) - \dot{u}_1(t)}{u_y}\left\{\bar{A} - |z(t)|^n[\beta_1 + \gamma_1 \text{sgn}((\dot{u}_{ext}(t) - \dot{u}_1(t)) \cdot z(t))]\right\}. \tag{3}$$

In this paper, among the multiple possible values for the parameters of the Bouc–Wen model, it is assumed that $\bar{A} = 1$, as in [36]. Quantities β_1 and γ_1 control the shape and size of the hysteretic loop [35] and are assumed as $\beta_1 = \gamma_1 = 0.5$, so that $\beta_1 + \gamma_1 = 1$ as in [37]. The two constraints $\beta_1 + \gamma_1 = 1$ and $\bar{A} = 1$ make the Bouc–Wen model equivalent to a strain-softening material. Moreover, under such specific choices, F_y, u_y, and ψ have specific physical meanings, and variable $z(t)$ takes values in the range $[-1, 1]$. The exponent n governs the abruptness of the transition between elastic and post-elastic branches and it is assumed as $n = 2$. For larger values of n, the Bouc–Wen model approaches the behavior of a bilinear model.

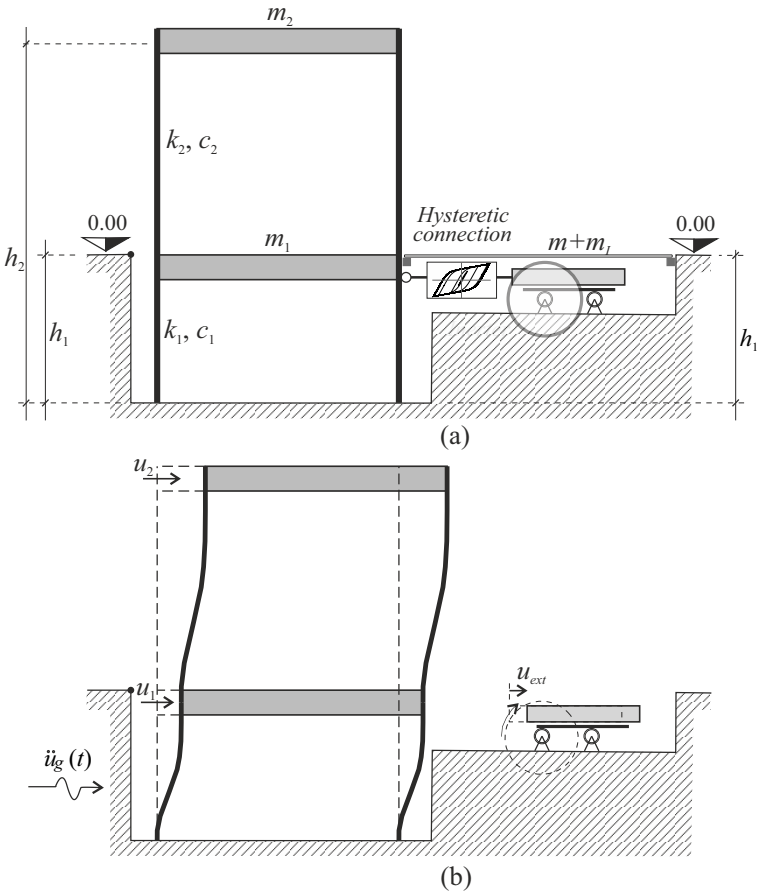


Figure 2. Coupled system: (**a**) geometrical and mechanical characteristics of the coupled system; (**b**) positive direction of the displacements u_1, u_2, and u_{ext}.

2.2. Inerter Device

The inerter is a device that applies a force F_{ID} proportional to the relative acceleration between its terminals. Among several types, the inerter can be constituted by a specific combination of rack–pinion flywheel devices, as seen in Figure 3. Two (or more) flywheels of radius R_i and mass $m_{\omega i}$, connected to a linear rack by a pinion-gear mechanism, are the main parts of such a device. The resisting force F_{ID} of the inerter device is [38,39]:

$$F_{ID} = m_I(\ddot{u}_{dx} - \ddot{u}_{sx}), \tag{4}$$

where m_I is the virtual mass (or inertance) of the inerter. The virtual mass of the device can be increased by adding other flywheels. When the inerter device is constituted by N flywheels, m_I reads

$$\begin{aligned} m_I = &\frac{1}{2}m_{\omega 1}\frac{R_1^2}{\rho_1^2} + \frac{1}{2}m_{\omega 2}\frac{R_1^2R_2^2}{\rho_1^2\rho_2^2} + \ldots + \frac{1}{2}m_{\omega i}\frac{R_1^2R_2^2\cdots R_i^2}{\rho_1^2\rho_2^2\cdots\rho_i^2} + \ldots + \\ &\frac{1}{2}m_{\omega N}\frac{R_1^2R_2^2\cdots R_i^2\cdots R_N^2}{\rho_1^2\rho_2^2\cdots\rho_i^2\cdots\rho_N^2}. \end{aligned} \tag{5}$$

The first two terms of Equation (5) provide the virtual mass m_I of the device in Figure 3. It should be noted that a kinetic energy exchange between the inerter and structure could occur with this kind of inerter device because there are no clutches (as in [38]) or similar devices to limit such an energy exchange.

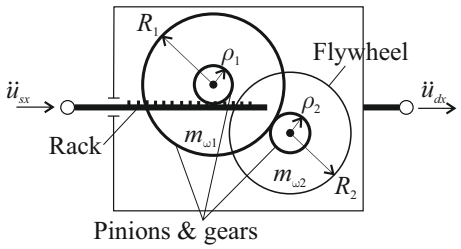


Figure 3. Rack–pinion flywheel rotational inertia system.

3. Parametric Analysis

This section presents the parameters varied in the parametric analyses. The parametric analyses aim to verify the effectiveness of the HMDI in improving the dynamic and seismic behaviors of frame structures in this paper.

3.1. Parameters Characterizing the HMDI

Among the parameters varied in the analyses, those characterizing the HMDI are the following:

- the ratio between the physical mass of the external structure m and the mass of the first story m_1

$$\gamma = \frac{m}{m_1}, \tag{6}$$

- the ratio between the virtual mass of the inerter m_I and the whole mass of the frame structure $m_1 + m_2$

$$\nu = \frac{m_I}{(m_1 + m_2)}, \tag{7}$$

- the ratio between the elastic stiffness k_c and the plastic stiffness k_{plast} of the hysteretic connection

$$\psi = \frac{k_{\text{plast}}}{k_c}, \tag{8}$$

- the ratio between the yielding forces $F_y = k_c u_y$ and the weight of the first story $m_1 g$

$$\beta_y = \frac{k_c u_y}{m_1 g}, \tag{9}$$

- the period T_{ext} of the stand-alone external oscillating mass

$$T_{ext} = 2\pi \sqrt{\frac{m + m_I}{k_c}}. \tag{10}$$

In Equation (9), g is the gravitational constant. The parameters γ and ν refer to the oscillating mass of the HMDI, ψ characterizes the hysteretic connection, and T_{ext} is the period of the stand-alone external oscillating mass. The period T_{ext}, which summarizes the behavior of the external mass, is obtained by assuming that the mass is linked directly to the ground with an elastic linear spring with stiffness k_c.

3.2. Parameters Characterizing the Frame Structure

In the parametric analyses, the 2-DOF model of the frame structure is used to describe three multi-story frame structures that have the characteristics reported in Table 1. For each multi-story frame structure, the mass and height of the stories are assumed to be constant at every level.

Table 1. Geometrical and mechanical characteristics of the three reference frame structures.

Stories	Connection Story	Floor Area	Story Mass m_s	Story Height
3	1	200 m^2	241.2×10^3 kg	3 m
4	1	250 m^2	301.5×10^3 kg	3 m
5	1	400 m^2	482.4×10^3 kg	3 m

By applying the dynamic equivalence criterion adopted in [18] to the frame structures in Table 1, it is possible to derive the characteristics of the low-dimensional 2-DOF models used in the analyses (Table 2).

Table 2. Dynamic characteristics of the 2-DOF equivalent models.

Stories	k_1 [Nm^{-1}]	k_2 [Nm^{-1}]	m_1 [kg]	m_2 [kg]
3	4.384382×10^8	1.879021×10^8	241.2×10^3	482.4×10^3
4	7.932988×10^8	2.440919×10^8	301.5×10^3	904.5×10^3
5	1.222606×10^9	2.910966×10^8	482.4×10^3	1929.6×10^3

3.3. Gain Parameters

Comparisons between the displacements and drifts (u_1 and $u_2 - u_1$) of the uncoupled and coupled frame structures (i.e., stand-alone frame structure and frame structure coupled with the protection device) are used to assess the ability of the HMDI to protect the structure against seismic excitation. As in Fabrizio et al.'s study [17], the two gain parameters are introduced as follows:

$$\alpha_1 = \frac{|u_{1\,\max}|}{|\tilde{u}_{1\,\max}|}, \; \alpha_2 = \frac{|(u_2 - u_1)_{\max}|}{|(\tilde{u}_2 - \tilde{u}_1)_{\max}|}, \tag{11}$$

where the displacements $\tilde{u}_1$ and $\tilde{u}_2$ are the displacements of the frame structure without the protection device. From the definition of the gain parameters in Equation (11), it can be observed that the lower the values of α_1 and α_2 are with respect to unity, the higher the dynamic protection provided by the HMDI.

4. Spectral Analysis

A spectral analysis is performed on the linearized homogeneous equations of motion of the coupled system. Such linearized equations are obtained by assuming that the restoring force F_H of the connecting device is linear, specifically, $F_H = k_c(u_{ext}(t) - u_1(t))$; such an expression is obtained from Equation (2) by letting $\psi = 1$. The linearized equations of the homogeneous coupled system can be expressed in matrix form as

$$\mathbf{M}\ddot{\mathbf{U}}(t) + \mathbf{K}\mathbf{U}(t) = \mathbf{0}, \tag{12}$$

where

$$\mathbf{K} = \begin{bmatrix} k_1 + k_2 + k_c & -k_2 & -k_c \\ -k_2 & k_2 & 0 \\ -k_c & 0 & k_c \end{bmatrix}, \quad \mathbf{M} = \begin{bmatrix} m_1 & 0 & 0 \\ 0 & m_2 & 0 \\ 0 & 0 & m + m_I \end{bmatrix}, \text{ and} \tag{13}$$

$$\mathbf{U}(t) = \begin{Bmatrix} u_1(t) \\ u_2(t) \\ u_{ext}(t) \end{Bmatrix}. \tag{14}$$

The corresponding frequencies and modes are obtained by solving the following eigenproblem:

$$(\mathbf{K} - \omega^2 \mathbf{M})\mathbf{\Phi} = \mathbf{0}, \tag{15}$$

where ω^2 is an eigenvalue of the system, and $\mathbf{\Phi}$ is the corresponding eigenvector.

4.1. Frequencies and Modal Shapes of the Coupled System

This section presents the analyses related to the four-story frame described in the second line of Table 1. The corresponding mechanical characteristics of the 2-DOF equivalent system are those in the second line of Table 2. Figure 4 shows how the periods and shapes of the oscillation modes of the frame structure change when it is coupled with the HMDI. Specifically, Figure 4a shows the periods and shapes of the two oscillating modes of the uncoupled structure, whereas Figure 4b shows the sketches of the three modes of the coupled system (provided by the 3-DOF equivalent system). For the coupled system, both periods and modal shapes are strictly related to the parameters of the mechanical system varied in the analyses. However, the modal shapes are less sensitive to such parameters. Specifically, the modal shapes of Mode 1 and Mode 3 remain qualitatively similar for all values of the system's parameters. On the contrary, the qualitative shape of Mode 2 changes, as explained below in detail.

The spectral analysis presented in this section aims to clarify the dependence of the dynamics of the coupled system on the characteristics of the frame structure and protection device. Figure 4c shows the values of the periods of the three modes as contour plots in the parameter plane ν–T_{ext}. It is worth remarking that the choice of ν (see Equation (7)) and T_{ext} (see Equation (10)) entails a combined variation of the linear elastic coupling stiffness k_c and virtual mass m_I. As can be observed by the contour levels of the period of Mode 1, the values of such a period strongly depend on ν (i.e., on the virtual mass m_I), since the contour levels are almost orthogonal to the ν-axis. Qualitatively, the period of Mode 1 increases when ν increases. The contour plots of the periods of Mode 2 and Mode 3 show that such periods are not significantly dependent on ν as that of Mode 1, especially for high values of ν. The main results can be summarized as follows:

- The period of Mode 1 can be increased using an appropriate virtual mass of the HMDI (i.e., increasing ν) so that it is possible to reach values significantly larger than those of the corresponding Mode $\hat{1}$ of the uncoupled frame structure.
- The period of Mode 2 of the frame coupled with the HMDI is consistently close to the period of Mode $\hat{1}$ of the uncoupled structure. It can be asserted that Mode 2 of the structure with the HMDI substitutes Mode $\hat{1}$ of the structure without the HMDI. Depending on the values of T_{ext} (i.e., depending on the characteristics of the HMDI), the shape of Mode 2 changes. In one case (Mode 2a), the HMDI moves in counter-phase with respect to the whole frame. In the other case (Mode 2b), the HMDI moves in phase with the first level of the frame structure and in counter-phase with the part of the structure above the connection with the HMDI. The threshold value that separates the regions of the parameter plane characterized by the two different modal shapes corresponds to a specific value $T_{ext} = \hat{T}_{ext}$ that exclusively depends on the characteristics of the uncoupled structure. In Figure 4c, such a value is $\hat{T}_{ext} = 0.382$ s and corresponds to the thick dashed line.

- The period of Mode 3 of the structure coupled with the HMDI always remains close to that of Mode $\hat{2}$ of the uncoupled structure. It can be asserted that Mode 3 of the coupled structure substitutes Mode $\hat{2}$ of the uncoupled structure.

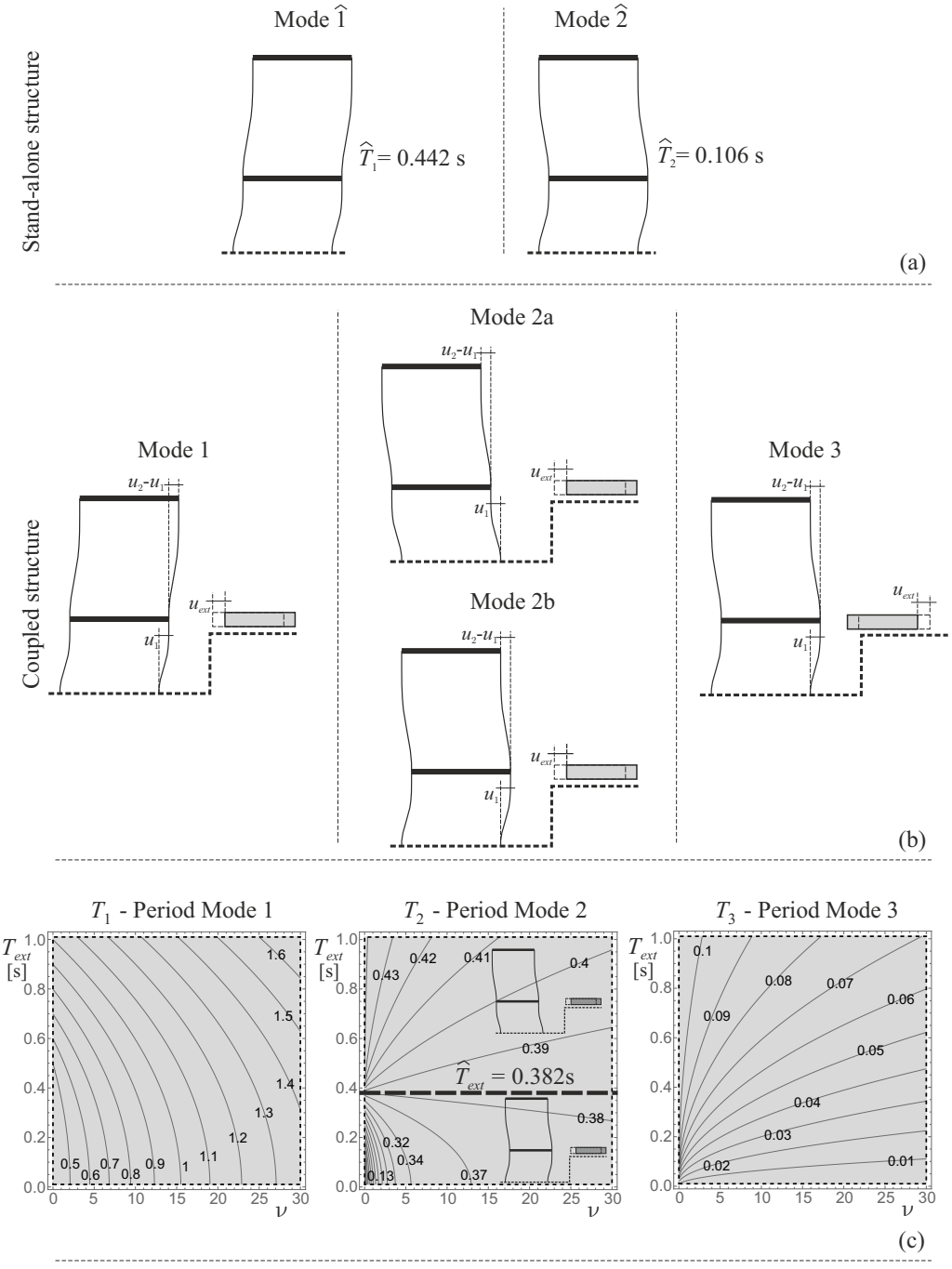


Figure 4. Spectral analysis of the uncoupled and coupled structures: (**a**) Periods and shapes of the modes of the uncoupled structure; (**b**) shapes of the modes of the coupled structure; (**c**) periods of the three modes of the coupled structure ($\gamma = 0.1$).

4.2. Modal Mass Participating Coefficients of the Coupled System

The values of the mass participating coefficients (MPCs) of the three modes of the structure with the HMDI provide insights into the dynamic effects of the coupling [40,41]. The modal participation factor is defined as $\tilde{\Gamma}_i = \mathbf{\Phi}_i \mathbf{M} \mathbf{r}$, where $\mathbf{\Phi}_i$ is the vector of the i-th mode $(i = 1, 2, 3)$, $\mathbf{M}$ is the mass matrix (see Equation (15)), and $\mathbf{r}$ is, in this case,

a unitary vector. The MPC of the i-th mode is the percentage of mass indicating the participation of the i-th mode to the total response and, in the general case, is defined as $\text{MPC}_i = (\tilde{\Gamma}_i^2 M_i / \mathbf{r}^T \mathbf{M} \mathbf{r}) \times 100$. In the case under investigation, the normalization of the modes is performed assuming $\mathbf{\Phi}_i \mathbf{M} \mathbf{\Phi}_i = 1$ and $\mathbf{\Phi}_i \mathbf{K} \mathbf{\Phi}_i = {\omega_i}^2$, and the values of the MPCs become $\text{MPC}_i = (\tilde{\Gamma}_i^2 / \mathbf{r}^T \mathbf{M} \mathbf{r}) \times 100$ because $M_i = 1$.

Figure 5 shows the contour maps of the values of the MPCs in the ν–T_{ext} parameter plane. The threshold value $\hat{T}_{ext} = 0.382$ s that corresponds to a change in the shape of Mode 2 is included in the contour maps of the MPCs of both Mode 1 and Mode 2 (left and middle graphs). It can be observed that the value of T_{ext} also corresponds to the minimum values of the MPCs of Mode 1 and Mode 2.

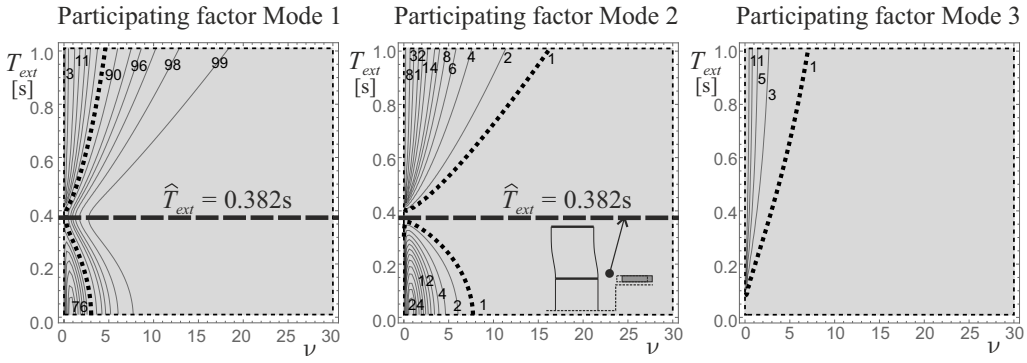


Figure 5. Spectral analysis of the coupled structures: modal mass participating factors of the three modes ($\gamma = 0.1$).

Analyzing the values in Figure 5, the following remarks can be made:

- The MPC of Mode 1 is higher than 90% (the dotted line refers exactly to 90%) in almost all of the parameter planes so that Mode 1 is largely the predominant oscillation mode. The dynamics associated with this mode do not reduce the displacements of the frame structure since the HMDI and the frame structure move in phase. However, the HMDI also has the effect of increasing the period of such a mode. In the case of seismic excitation, the increase of the prevailing period has a protective effect on the structures because earthquakes have lower spectral energy in the range of higher periods. The shifting of the period of the prevailing mode toward higher values is the same protection concept at the base of base isolation.
- The MPC of Mode 2 is less than 1% (the dotted line refers to 1%) in almost all the parameter planes. Therefore, although the introduction of the HMDI has the effect of substituting Mode $\hat{1}$ of the uncoupled structure with Mode 2 (i.e., the two modes before and after the coupling with the protection device have close values to the period), it also reduces the participation mass of this mode. Consequently, it reduces the influence that this mode would have under seismic excitation, considering that the period of Mode 2 is usually in the range of values where earthquakes have higher spectral energy. The contour map of the MPC of Mode 2 also shows the shape of the mode obtained at the threshold value $\hat{T}_{ext}$. The shape indicates that there is no displacement at the first level of the 2-DOF system. Therefore, it is expected that the dynamics associated with this mode minimize the displacement u_1.
- From observing the shapes of Mode 2a and Mode 2b, it can be expected that the protection device has the main effect of reducing u_1 (i.e., the displacement of the story connected to the HMDI) when the design parameter T_{ext} is higher than $\hat{T}_{ext}$, because the story where the connection is placed and the HMDI move in counter-phase. On the other hand, when T_{ext} is less than $\hat{T}_{ext}$, the use of the protection device leads to a reduction of the drift ($u_2 - u_1$) because, in this case, the upper part of the frame structure and the HMDI move in counter-phase.
- In general, it can be stated that, in the coupled structure, the modal displacement of the HMDI u_{ext} is larger than u_1 and $u_2 - u_1$ in all three modes. Moreover, u_{ext} increases

compared to u_1 and $u_2 - u_1$ when either ν or T_{ext} increase. It can also be asserted that the HMDI directs the external excitation on itself, thus reducing the dynamic effect on the structure, i.e., leading to smaller displacements than in the case of the uncoupled structure.

5. Seismic Analysis

The analysis discussed in this section aims to verify if the HMDI improves the seismic response of frame structures under seismic excitation. Two different types of seismic excitation are considered: (i) single earthquake records and (ii) a set of seven spectrum-compatible earthquake records.

5.1. Single Earthquake Records and Set of Spectrum-Compatible Earthquake Records

In the first set of seismic analyses, three different earthquake records, selected by taking into account their spectral characteristics, are used as the base excitation. The recorded time histories and the pseudo-acceleration elastic spectra of such records are shown in Figure 6. Specifically, the chosen ground records are:

(a) Kobe, 1995 Japan earthquake, Takarazuka station, 0 deg, ground level, position of the station: 34.8090 N, 135.3440 W;
(b) Northridge, Newhall, 1994 California earthquake,- LA County Fire station no. 24279, 360 deg, position of the station: 34.387 N, 118.530 W;
(c) Parkfield, 1966 California earthquake, station no.013, comp N65 E, position of the station: 35.726 N, 120.287 W.

In the above list, the underlined names are used to refer to the specific earthquake records.

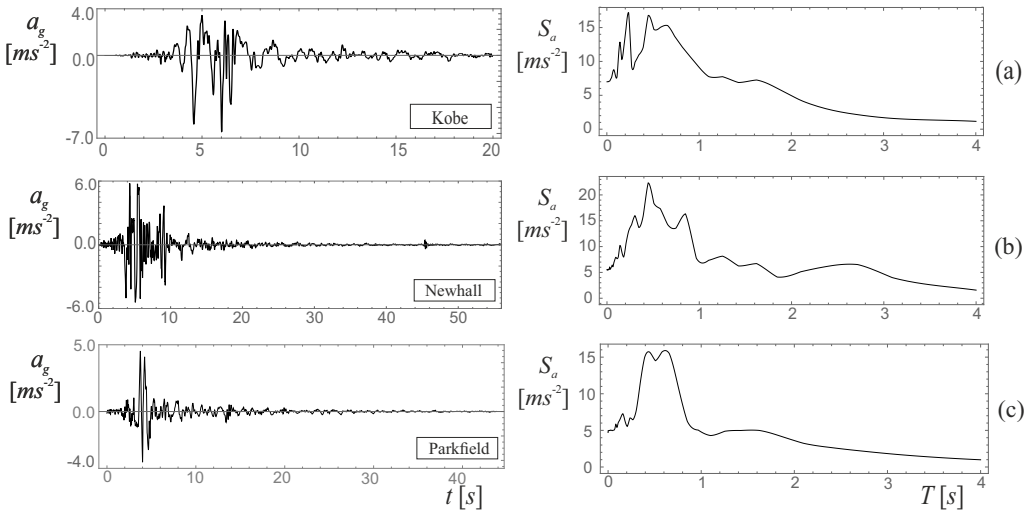


Figure 6. Time histories and acceleration response spectra of the earthquakes analyzed: (**a**) Kobe; (**b**) Newhall; (**c**) Parkfield.

In a second set of seismic analyses, seven earthquake records are instead used to meet the spectrum-compatibility criterion. According to the Italian Technical Building Codes (NTC 2018), the spectrum compatibility requires that the mean value of spectral ordinates obtained from a group of at least seven earthquake records must not be lower than 10% of the design spectrum for each period in a specific range. The seven earthquake records used in this study are selected to be compatible with the design spectrum of Los Angeles, according to the ASCE7-10 rules. The main characteristics of the seven records are reported in Table A1 of Appendix A. The horizontal design spectrum accounts for an "A" class site and a category *III* risk (in particular, the design parameters are $T_L = 8$ s, $S_s(g) = 2.432$ g, and $S_1 = 0.853$). The earthquake records are selected using the software Rexel [42]. The parameter selection is carried out considering values of the magnitude and epicentral

distance consistent with seismic hazards at the specific site. Figure 7 shows the spectra of each earthquake record (thin lines), the target spectrum (thick line), and the average spectrum (dashed thick line).

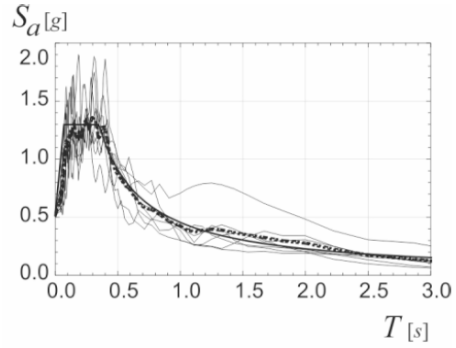


Figure 7. Spectra of the selected set of seven earthquakes, (dashed, solid thick, and solid thin lines refer to the average spectrum, the design spectrum, and the record spectra, respectively).

5.2. Spectral Gain Curve of a Single Seismic Event

The first set of analyses aims to obtain the spectral gain curves using a single seismic record. These curves provide the values of one gain coefficient, either α_1 or α_2, versus T_{ext}. All the spectra presented in this section are for the 4-story frame structure with mechanical characteristics reported in the second lines of Tables 1 and 2.

Within this set of analyses, the first investigation is performed by varying the parameter ψ, which characterizes the post-elastic behavior of the hysteretic connection. Figure 8 shows the gain spectra of α_1 (left graphs) and α_2 (right graphs) for the Kobe (first line of the graphs) and Newhall (second line of the graphs) earthquake records. The spectra are obtained for fixed values of $\nu = 10$, $\beta_y = 1.5$, and $\gamma = 0.1$. It is important to note that, by fixing γ and ν (and thus m and m_I), a variation of the parameter T_{ext} corresponds to a variation of the elastic stiffness k_c only. Each graph contains two spectra, one obtained for $\psi = 1$ (thin line) and the other for $\psi = 0.1$ (thick line). The value of $\psi = 1$ refers to a connection device that has a linear elastic behavior with a stiffness k_c (see Equation (2)). Each graph includes a horizontal dashed line passing through the unitary value of the relevant gain coefficient. According to the definition of the gain coefficients in Equation (11), if the spectrum lies below the unitary line, then the HMDI is effective in reducing the displacements of the frame structure. On the other hand, if the spectrum is above the unitary line, the displacements of the coupled structure are larger than those of the uncoupled structure, and the coupling with the HMDI does not provide any benefits to the structure. It is worth noting that the presence of an external oscillating mass improves the seismic behavior of the structure, both in the case of elastic ($\psi = 1$) and hysteretic ($\psi = 0.1$) connections since the gain spectra are below the unitary horizontal line in almost all the investigated range of T_{ext}. The case with $\psi = 1$ corresponds to a classical Tuned Mass Damper Inerter (TMDI) [26–28,31]. The comparison between the spectra obtained for $\psi = 1$ and $\psi = 0.1$ reveals that the hysteretic behavior of the connection ($\psi = 0.1$) results in reduced values of the gain coefficients in almost all the range of T_{ext} (i.e., the HMDI is effective in reducing the displacements of the frame structure) and an increase in the range of values of T_{ext} where α_1 decreases compared to the case of a linear elastic connection ($\psi = 1$).

It is noteworthy that in all cases, the spectra have points of absolute minimum where the reduction of displacements is maximized. As shown before, the minimum point of the α_1 spectrum is located close to $\hat{T}_{ext}$. Conversely, the value $\hat{T}_{ext}$ does not represent a point of particular interest for the α_2 spectra, but it is expected that the absolute minimum of α_2 occurs for values of T_{ext} less than $\hat{T}_{ext}$.

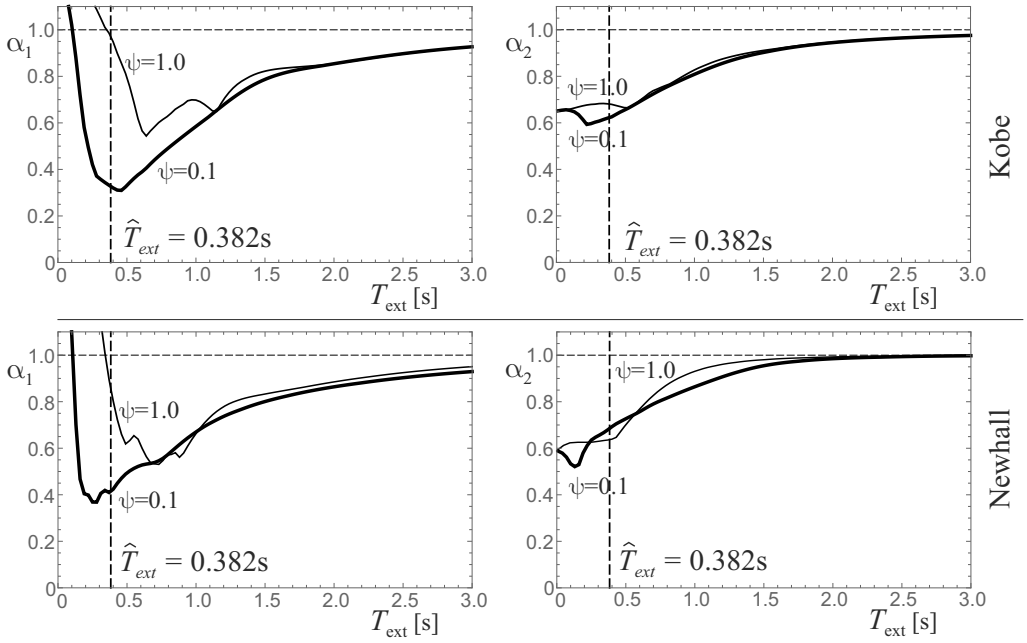


Figure 8. Spectral gain curve of the four-story frame structure under Kobe and Newhall earthquakes: parameter ψ variable (thick line: $\psi = 0.1$; thin line: $\psi = 1.0$; $\nu = 10$; $\beta_y = 1.5$; $\gamma = 0.1$).

A further analysis investigates the role of the parameter β_y, which defines the threshold between the elastic and plastic behavior of the hysteretic connection. Figure 9 shows the gain spectra of α_1 (left graphs) and α_2 (right graphs), referring to the Kobe (first line of graphs) and Newhall (second line of graphs) earthquake records. The spectra are obtained for fixed values of $\nu = 10$, $\psi = 0.1$, and $\gamma = 0.1$. Each graph contains four spectra related to different values of β_y, ranging from 0.2 to 3.0, as indicated in the graphs. In particular, in the graphs, the dashed line refers to the spectrum with the highest value of $\beta_y = 3.0$. The increase of β_y from 0.2 to 1.5 is associated with an improvement in the performance of the system because the values of both α_1 and α_2 monotonically reduce (thus, confirming a decrease in the displacements of the frame structure). Such a reduction stops for $\beta_y = 3.0$ and the spectra referring to $\beta_y = 3.0$ show ranges of T_{ext}, where α_1 and α_2 have larger values than those obtained for $\beta_y = 1.5$. The increase in the displacements of the coupled system for β_y above a threshold value can be explained by noting that the increase in β_y corresponds to an increase in the yielding force F_y (or, equivalently, in the yielding displacement u_y, as given by Equation (2)). When F_y becomes significantly large, the system is unable to reach the yielding point of the connection device, which therefore behaves as a linear elastic element. Moreover, in such cases, the spectra of α_1 exhibit points of absolute minimum near $\hat{T}_{ext}$.

In this section, the physical mass of the HMDI m is the last parameter whose influence on the dynamics of the coupled system is investigated. Figure 10 shows the gain spectra of α_1 (left graphs) and α_2 (right graphs), referring to the Kobe (first line of graphs) and Newhall (second line of graphs) earthquake records. The spectra are obtained for fixed values of $\beta_y = 1.5$ and $\psi = 0.1$. Each graph contains two spectra, one obtained for $m_I = 10(m_1 + m_2)$ and $m = 0.1m_1$ (thick line) and the other obtained for $m_I = 0.1m_1$ and $m = 10(m_1 + m_2)$ (thin line). Specifically, the thick curves refer to the spectra obtained by considering values of the virtual mass m_I much larger than those of the physical mass m. On the contrary, the thin curves represent spectra where m has larger values than m_I. It can be observed that using virtual mass instead of physical mass (i.e., using an inerter device instead of increasing the physical mass of the protection device) significantly enhances the performance of the HMDI, especially in reducing the displacement of the first story (represented by the α_1 spectral curves).

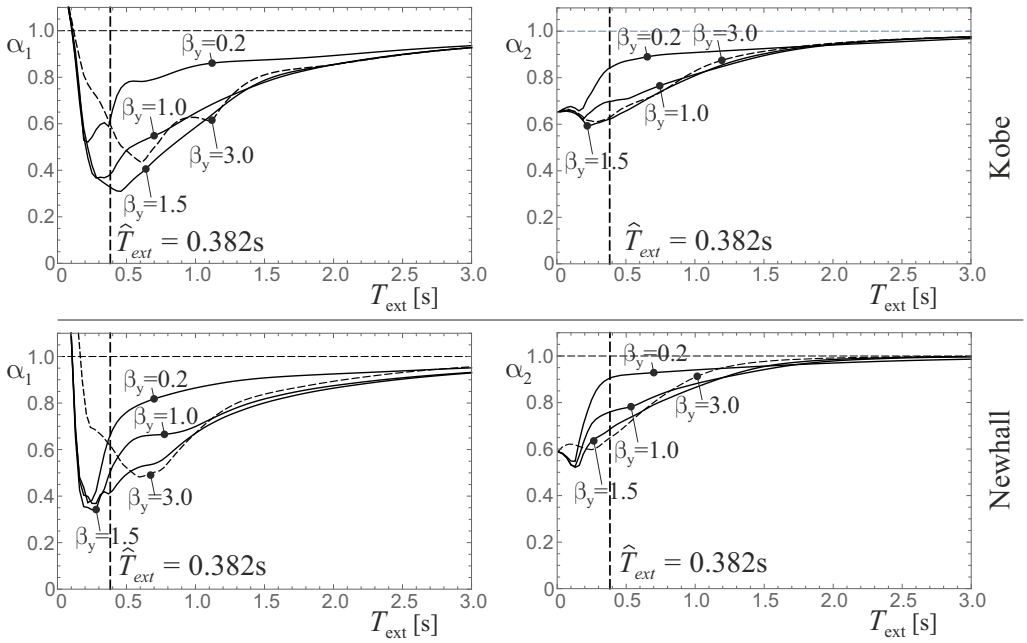


Figure 9. Spectral gain curve of the four-story frame structure under Kobe and Newhall earthquakes: parameter β_y variable ($\nu = 10$; $\psi = 0.1$; $\gamma = 0.1$).

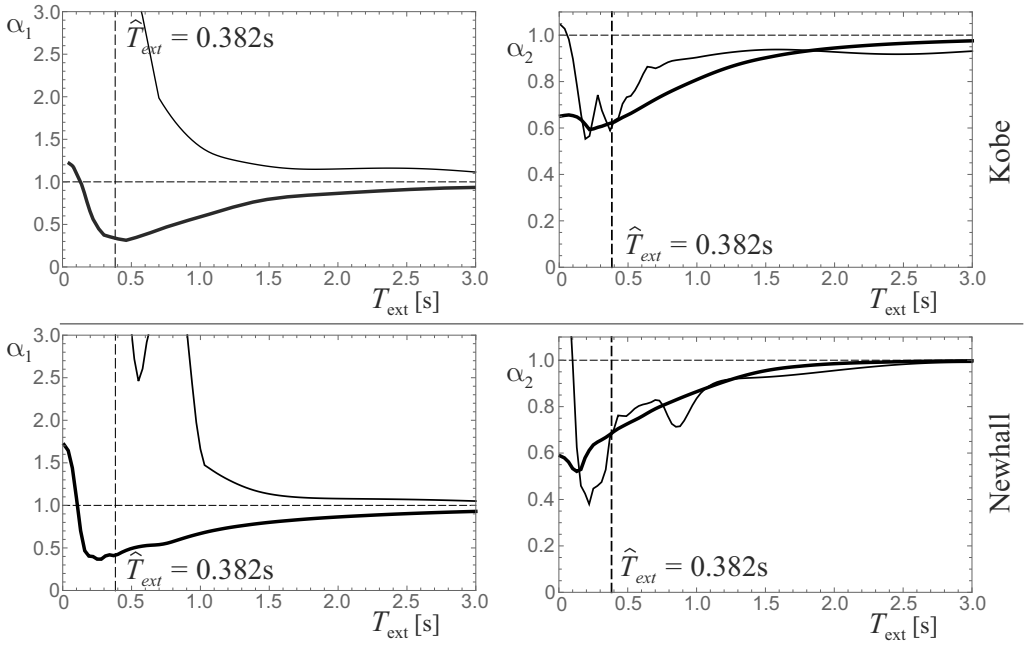


Figure 10. Spectral gain curve of the four-story frame structure under Kobe and Newhall earthquakes: parameters m and m_I variable (thick line: $m_I = 10(m_1 + m_2)$, $m = 0.1m_1$; thin line: $m_I = 0.1m_1$, $m = 10(m_1 + m_2)$); ($\beta_y = 1.5$; $\psi = 0.1$).

5.3. Spectral Gain Maps of a Single Earthquake Record

This section presents the results of an analysis performed to obtain the spectral gain maps of the coupled structure under a single earthquake record. Such maps are contour plots of one gain coefficient, either α_1 or α_2, in the parameter plane ν–T_{ext}. As in the previous analyses, all other parameters characterizing the coupled system are fixed. In these gain maps, the light gray regions are those where the gain coefficient is smaller than unity; thus, these are regions where the HMDI reduces u_1 or $u_2 - u_1$, compared with those of the uncoupled structure. On the contrary, the dark gray regions are those where the gain

coefficient is higher than unity. It is worth noting that the sections of the gain maps parallel to the T_{ext} axis are the spectral gain curves described in the previous section.

Figure 11 shows the gain maps of α_1 (left column) and α_2 (right column) refers to the four-story frame structure (see Tables 1 and 2), which is excited by the three earthquake records, i.e., Kobe (first row), Newhall (middle row), and Parkfield (third row). As can be observed, the advantage regions where the gain coefficients are smaller than unity (light gray regions) cover almost all of the parameter plane ν–T_{ext}. Each map in Figure 11 shows a thick dashed line representing the value of $\hat{T}_{ext}$. From the gain maps of the Kobe earthquake (first row), it can be observed that the lowest values of α_1 can be found for $T_{ext} = \hat{T}_{ext}$. The same does not occur for α_2; the lowest values of α_2 can be found for $T_{ext} < \hat{T}_{ext}$, as anticipated in the previous sections. The other two earthquake records lead to similar results. Specifically, when the Newhall and Parkfield earthquake records are considered, the lowest values of α_1 are not in correspondence with $\hat{T}_{ext}$ but can be obtained for values of T_{ext} that are slightly lower than $\hat{T}_{ext}$. Moreover, for these two additional earthquake records, the lowest values of α_2 are found for $T_{ext} < \hat{T}_{ext}$. The contour levels of the gain maps show that the HMDI significantly reduces the displacement of the story connected to the HMDI and/or the drift of the upper stories. Since the regions where α_1 and α_2 take the lowest values do not coincide, it is not possible to obtain design parameters that simultaneously minimize u_1 and $u_2 - u_1$. However, it is always possible to choose design parameters where both α_1 and α_2 are smaller than unity.

It is important to note that, in the maps, the position of the lowest value of α_1 with respect to $\hat{T}_{ext}$ depends on the seismic record and, in particular, on its frequency spectral content. For instance, considering the Kobe earthquake record, the lowest values of α_1 are obtained for values of T_{ext} that are significantly close to $\hat{T}_{ext}$, whereas using the Newhall and Parkfield earthquake records the lowest values of α_1 are obtained for values lower than T_{ext}.

Figure 12 shows time histories used to investigate the interaction between the frame structure and HMDI further. The graphs are arranged in four rows, each referring to one of the points labeled from A to D in the gain maps obtained with the Kobe and Newhall earthquake records (Figure 11). The graphs in the first row refer to point A ($\nu = 13.0; T_{ext} = 0.4$ s), which is very close to the point of minimum value of α_1. Moreover, point A is obtained for a value of T_{ext} slightly larger than $\hat{T}_{ext}$, thus corresponding to the shape of the second oscillation mode named Mode 2a (see Figure 4). In such a mode, both the modal displacements u_1 and $u_2 - u_1$ are in counter-phase with the modal displacement u_{ext} of the HMDI. Therefore, if the seismic record excites the second mode due to its spectral content, the motion of the frame structure and the HMDI should not be in phase. The left and middle graphs compare the time histories of u_1 and u_{ext} (left graph) and $u_2 - u_1$ and u_{ext} (middle graph), respectively. In this case, the motion of the HMDI, represented by u_{ext} (dashed line), is primarily in counter-phase with both u_1 and $u_2 - u_1$, especially when the drift is larger.

The graphs in the second row refer to point B ($\nu = 4.5; T_{ext} = 0.175$ s), which corresponds to a value of T_{ext} that is slightly smaller than $\hat{T}_{ext}$ and, consequently, to the second oscillation mode, named Mode 2b (see Figure 4). In such a mode, u_1 is in phase with u_{ext}, while $u_2 - u_1$ and u_{ext} are in counter-phase with u_{ext}. Moreover, for point B, the left and middle graphs compare the time histories of u_1 and u_{ext} (left graph) and $u_2 - u_1$ and u_{ext} (middle graph).

The graphs on the third and fourth lines refer to points C ($\nu = 12.0; T_{ext} = 0.2$ s) and D ($\nu = 3.0; T_{ext} = 0.125$ s), respectively. Such points correspond to values of T_{ext} that are smaller than $\hat{T}_{ext}$ (i.e., to Mode 2b shown in Figure 4). The left and middle graphs show that the motion of the HMDI, (dashed line) is fundamentally in phase with u_1 and in counter-phase with $u_2 - u_1$. In the right graphs of each row, the hysteretic cycles of the connection device show that the largest energy dissipation (i.e., the larger equivalent damping) is associated with the point with the minimum value of α_1.

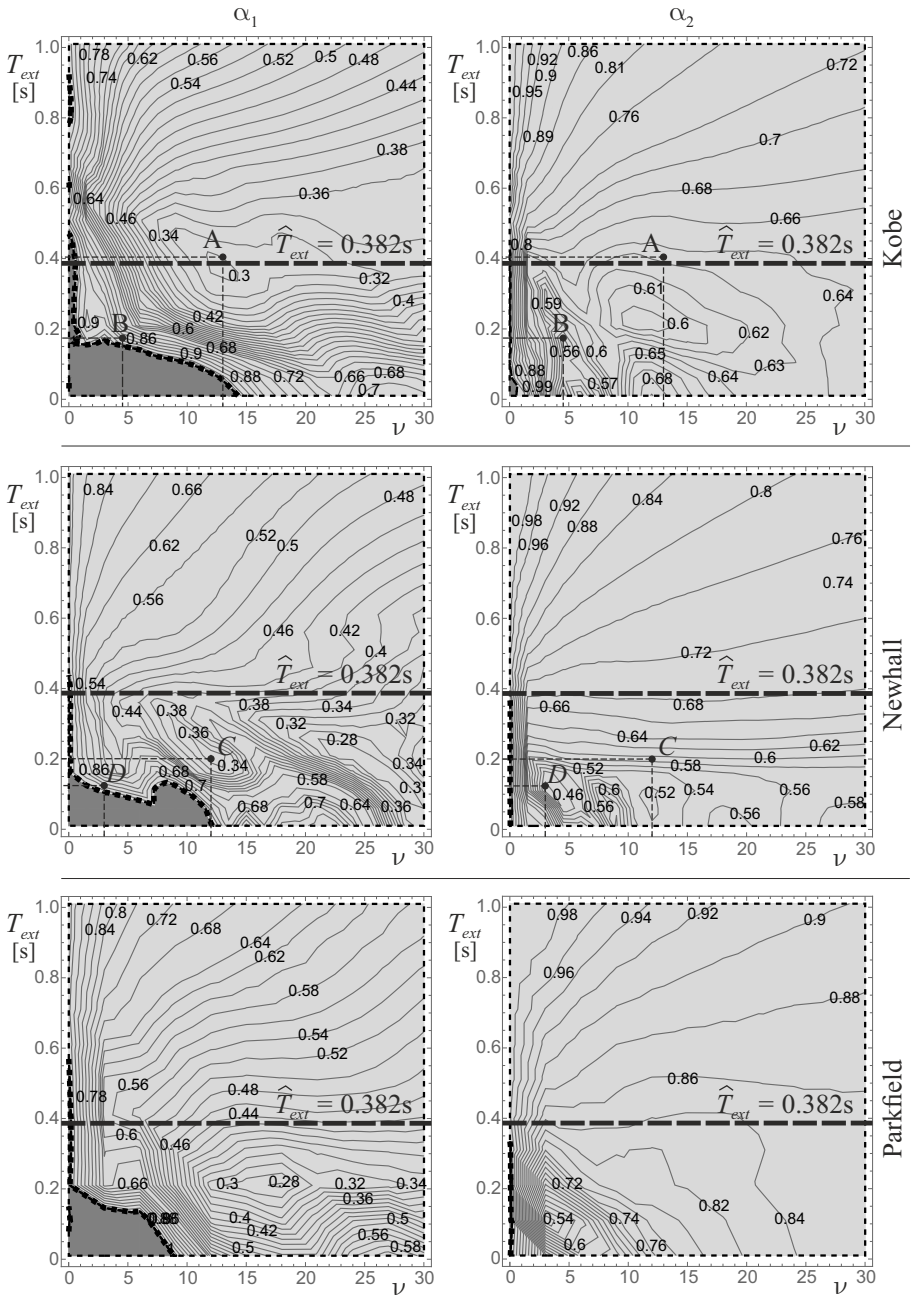


Figure 11. Spectral gain maps of the four-story frame structure under Kobe, Newhall, and Parkfield earthquakes ($\beta_y = 1.5$; $\gamma = 0.1$; $\psi = 0.1$).

To conclude, Figure 13 shows the gain maps of the three- (first row) and five-story (second row) frame structures (see Tables 1 and 2 for the characteristics), excited by the Parkfield earthquake record. The coupling with the HMDI is effective for these two frame structures. Nevertheless, the effectiveness of the HMDI reduces when coupled to the five-story frame structure if compared to shorter frame structures, i.e., the values of α_1 and especially those of α_2 are generally larger than those obtained for the three-story frame structure. Finally, it is worth noting that for these two frame structures, the values $\hat{T}_{ext}$ are different from the values considered for the four-story frame structures used in most of the analyses because the value of $\hat{T}_{ext}$ depends on the characteristics of the uncoupled structure.

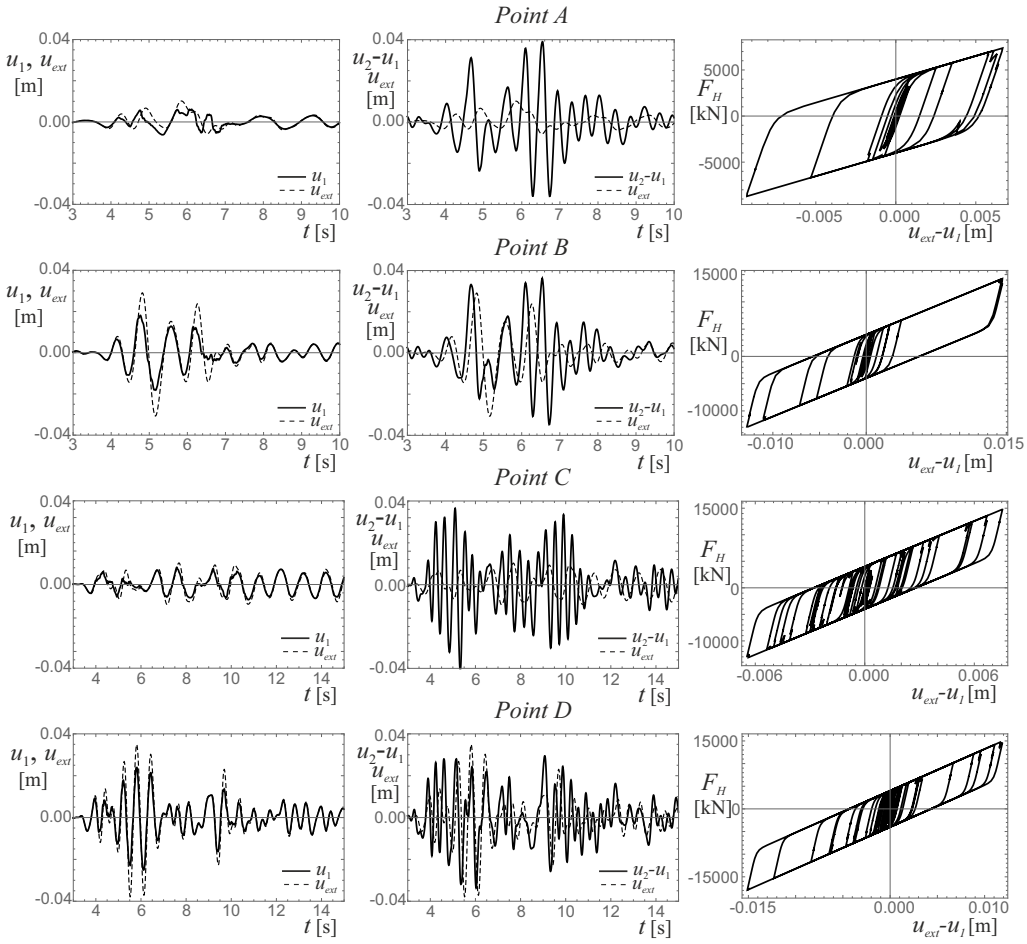


Figure 12. Time histories and hysteretic cycles at points A ($\nu = 13, T_{ext} = 0.375$), B ($\nu = 4.5$, $T_{ext} = 0.175$), C ($\nu = 12, T_{ext} = 0.2$), and D ($\nu = 3, T_{ext} = 0.125$), shown in Figure 11 ($\beta_y = 1.5$; $\gamma = 0.1$; $\psi = 0.1$).

5.4. Spectral Gain Maps of a Set of Spectrum-Compatible Earthquake Records

In this section, the formulation of the gain parameters in Equation (11) is adjusted to consider that the analysis is conducted using a group of seven earthquake records that are compatible with an assumed spectrum. Specifically,

$$\bar{\alpha}_1 = \frac{\sum_{i=1}^{n} \max[u_{1i}(t)]}{\sum_{i=1}^{n} \max[\tilde{u}_{1i}(t)]}; \quad \bar{\alpha}_2 = \frac{\sum_{i=1}^{n} \max[u_{2i}(t) - u_{1i}(t)]}{\sum_{i=1}^{n} \max[\tilde{u}_{2i}(t) - \tilde{u}_{1i}(t)]} \tag{16}$$

where $n = 7$ is the number of earthquake records used to build the spectrum. The analysis aims to obtain spectrum-compatible gain maps that are contour plots of one gain coefficient, either $\bar{\alpha}_1$ or $\bar{\alpha}_2$, in the parameter plane ν–T_{ext}, for fixed values of all of the other parameters. Moreover, for the maps, the light gray regions are those where the gain coefficients are smaller than unity, i.e., where the HMDI is effective, whereas dark gray regions refer to gain coefficients higher than unity.

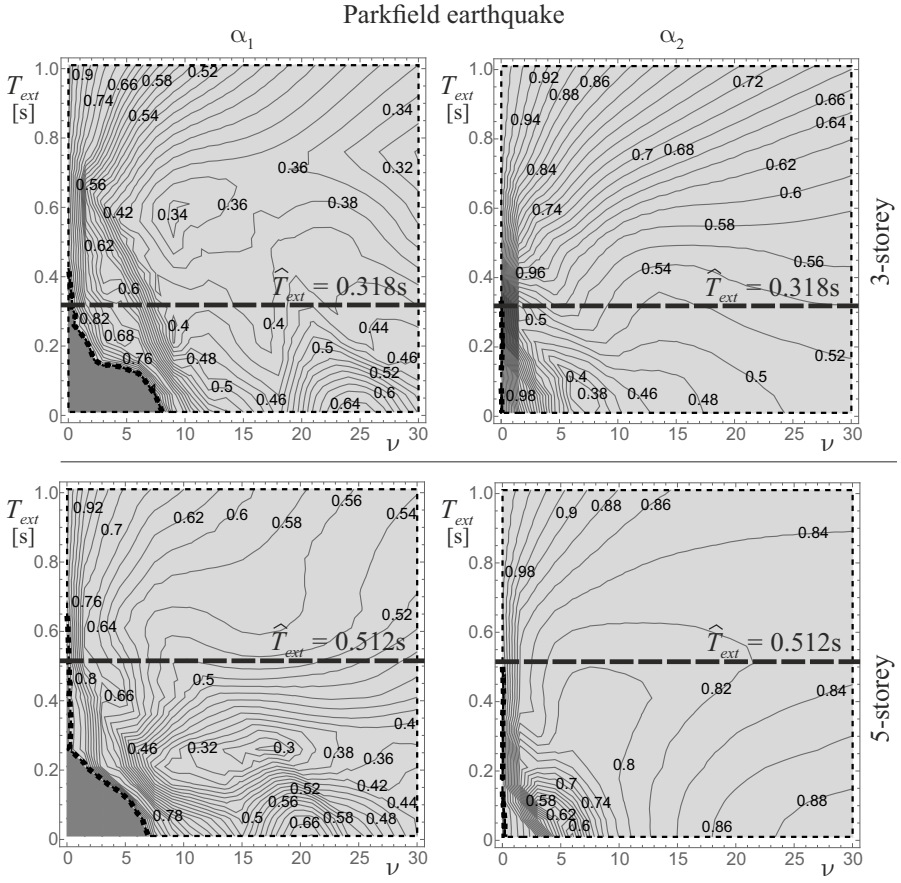


Figure 13. Spectral gain maps of the three- and five-story frame structures under Parkfield earthquakes ($\beta_y = 1.5$; $\gamma = 0.1$; $\psi = 0.1$).

Figure 14 shows the spectrum-compatible gain maps of the three-story (first row) and five-story (second row) frame structures. As intended, such maps significantly depend on the chosen design spectrum and only slightly on the specific seven earthquake records used in the analysis. The HMDI is effective for the three-story frame structure, resulting in a noticeable reduction of both u_1 and $u_2 - u_1$. On the other hand, the maps of the five-story frame structure present wider dark gray regions (no advantage regions) than the gain maps of the three-story frame structure. Moreover, within the light gray regions, the values of α_1 and especially α_2 are significantly higher than those obtained for the three-story frame structure. Such reduced effectiveness for the five-story frame structure highlights a limitation of the proposed protection method based on the use of HMDI because the performance of the coupling with the HMDI reduces for taller frame structures. The reason is that, having fixed the level of the connection with the HMDI at the first story, the HMDI is effective only if the number of stories above the connection level is sufficiently small. Therefore, the proposed method is mostly effective for low- and medium-rise frame structures. Theoretically, such a limitation could be removed by extending or transferring the effects of the HMDI to higher intermediate stories, and this possibility should be studied in detail.

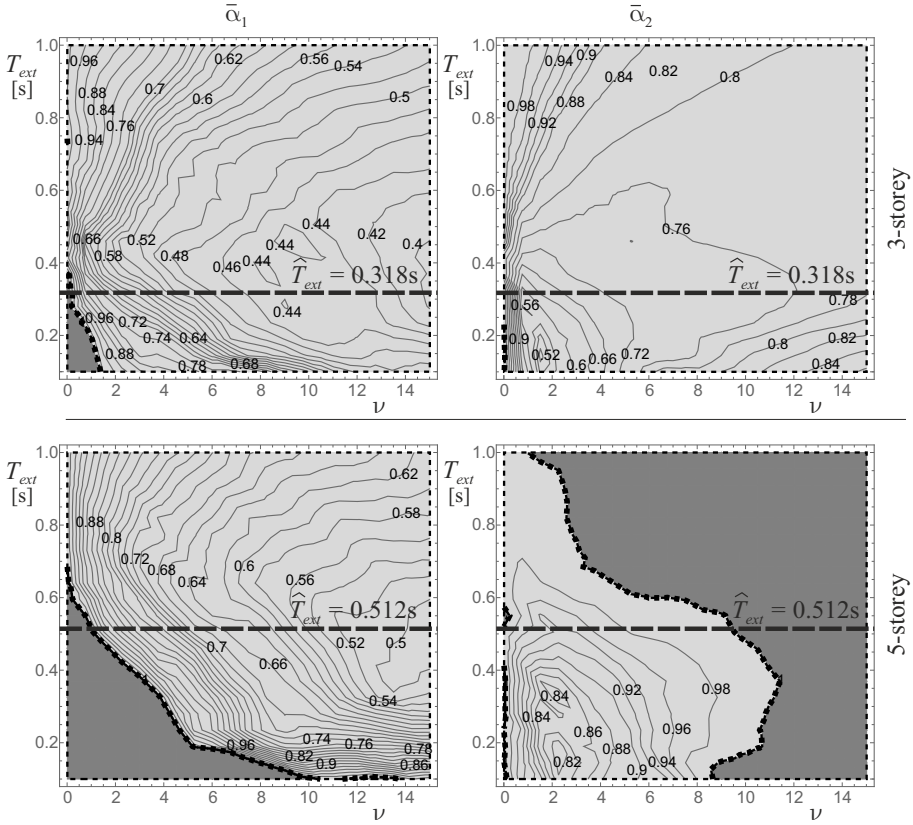


Figure 14. Spectral gain maps of the three- and five-story frame structures under spectrum-compatible seismic records with the Los Angeles design spectrum ($\beta_y = 1.5$; $\gamma = 0.1$; $\psi = 0.1$).

6. Conclusions

In this paper, the connection between a multi-story frame structure and an external oscillating mass is investigated with the aim to improve the seismic behavior of the frame structure. The frame structure is modeled with a two-degree-of-freedom system, whereas the external mass is described by a single-degree of-freedom-system. The external mass is connected at the first story of the frame structure through a hysteretic device and its inertial force is increased by means of an inerter device. The whole protection device, i.e., the external body together with the hysteretic connection and inerter device, is named "hysteretic mass damper inerter". The coupled structure, consisting of the frame structure and protection device, is modeled as a three-degree-of-freedom (3-DOF) mechanical system. The equations of motion are derived using a direct approach.

A preliminary spectral analysis is conducted using the linearized mechanical system to study the dynamics of the coupled system. Results indicate that the HMDI increases the period of the main mode of the coupled system, which is similar to the effect of base isolation. Additionally, the modal mass participating coefficient (MPC) of the main mode increases up to 90% in most practical cases. It is also demonstrated that the period of the HMDI, evaluated as if it was directly connected to the ground (i.e., studying the relative one-degree-of-freedom model), is one of the most important parameters that determine the effectiveness of the HMDI. The value of such parameter is directly related to the shape of the second oscillating mode of the coupled system, which replaces the main mode of the stand-alone frame structure. By suitably choosing this parameter, it is possible to increase the effectiveness of the HMDI and reduce the displacement at the connection level and the inter-story drift.

After the spectral analysis, a seismic analysis is conducted using three ground motion records or a set of seven earthquake records compatible with the spectrum of Los Angeles. Two gain coefficients are used to evaluate the effectiveness of the HMDI. Such gain coefficients provide the ratios between the corresponding displacements of the coupled and

stand-alone frame structures. Gain coefficients smaller than unity indicate the effectiveness of the HMDI in reducing displacements and drifts. Results are presented in spectral gain maps, which are contour plots of the gain coefficients in specific parameter planes. It is found that there are large ranges of the parameters characterizing the HMDI where the protection device is effective in the reduction of the displacement of the first story and the drift of the upper stories of the frame structure. Moreover, it is found that the HMDI is particularly effective in low- and medium-rise frame structures.

Author Contributions: All authors contributed equally to this work. All authors have read and agreed to the published version of the manuscript.

Funding: This research received no external funding.

Data Availability Statement: The data presented in this study are available on request.

Conflicts of Interest: The authors declare no conflict of interest.

Appendix A. Spectrum Compatibility Earthquake Records

Table A1 shows the list of spectrum compatibility seismic records for Los Angeles. In particular, W.ID and E.ID are the identification codes of the waveform and the earthquake use in the software Rexel [42]; StationID is the identification code of the station that acquired the record, Mw denotes the magnitude of the seismic event, FaultM provides a brief description of the fault mechanism, and Epic represents the epicentral distance in kilometers.

Table A1. Set of seven seismic records selected to be compatible with the design spectrum of Los Angeles (USA), accordingly to ASCE7-10 rules.

W.ID	E.ID	Name	Station ID	Date	Mw	FaultM	Epic
6263	1635	South Iceland	ST2484	17/06/2000	6.5	strike-slip	7
292	146	Campano Lucano	ST98	23/11/1980	6.9	normal	25
1314	474	Ano Liosia	ST1101	07/09/1999	6.0	normal	17
7142	2309	Bingol	ST539	01/05/2003	6.3	strike-slip	14
1708	474	Ano Liosia	ST1253	07/09/1999	6.0	normal	19
6335	2142	South Iceland (aftershock)	ST2557	21/06/2000	6.4	strike-slip	15
4674	1635	South Iceland	ST2486	17/06/2000	6.5	strike-slip	5

References

1. Kelly, J. Base isolation: Linear theory and design. *Earthq. Spectra* **1995**, *6*, 223–244. [CrossRef]
2. Den Hartog, J.P. *Mechanical Vibrations*, 4th ed.; McGraw-Hill: New York, NY, USA, 1956.
3. Rana, R.; Soong, T. Parametric analysis and simplified design of tuned mass damper. *Eng. Struct.* **1998**, *20*, 193–204. [CrossRef]
4. Miranda, J.C. On tuned mass dampers for reducing the seismic response of structures. *Earthq. Engng. Struct. Dyn.* **2005**, *34*, 847–865. [CrossRef]
5. Tsai, H.H. The effect of tuned-mass dampers on the seismic response of base-isolated structures. *Int. J. Solid Struct.* **1995**, *32*, 1195–1210. [CrossRef]
6. Taniguchi, T.; Kiureghian, A.D.; Melkumyan, M. Effect of tuned mass damper on displacement demand of base-isolated structures. *Eng. Struct.* **2008**, *30*, 3478–3488. [CrossRef]
7. Bachmann, J.; Vassiliou, M.; Stojadinović, B. Dynamics of Rocking Podium Structures. *Earthq. Eng. Struct. Dyn.* **2017**, *46*, 2499–2517. [CrossRef]
8. Makris, N. A half-century of rocking isolation. *Earthqu. Struct.* **2014**, *7*, 1187–1221. [CrossRef]
9. Makris, N.; Aghagholizadeh, M. The dynamics of an elastic structure coupled with a rocking wall. *Earthq. Eng. Struct. Dyn.* **2017**, *46*, 945–954. [CrossRef]
10. Di Egidio, A.; Pagliaro, S.; Fabrizio, C. Combined use of rocking wall and inerters to improve the seismic response of frame structures. *J. Eng. Mech.* **2021**, *147*, 04021016. [CrossRef]
11. Di Egidio, A.; Pagliaro, S.; Fabrizio, C.; de Leo, A. Seismic performance of frame structures coupled with an external rocking wall. *Eng. Struct.* **2020**, *224*, 111207. [CrossRef]

12. Pagliaro, S.; Aloisio, A.; Di Egidio, A.; Alaggio, R. Rigid block coupled with a 2 d.o.f. system: Numerical and experimental investigation. *Coupled Syst. Mech.* **2020**, *6*, 539–562.
13. Di Egidio, A.; Pagliaro, S.; Contento, A. Seismic benefits of deformable connections between a frame structure and an external structure with inerter. *Eng. Struct.* **2022**, *256*, 113025. [CrossRef]
14. Di Egidio, A.; Pagliaro, S.; Contento, A. Elasto-plastic short exoskeleton to improve dynamic and seismic performances of frame structures. *Appl. Sci.* **2022**, *12*, 10398. [CrossRef]
15. Simoneschi, G.; Olivieri, C.; de Leo, A.; Di Egidio, A. Pole placement method to control the rocking motion of rigid blocks. *Eng. Struct.* **2018**, *98*, 154–162. [CrossRef]
16. Di Egidio, A.; Contento, A.; Olivieri, C.; de Leo, A. Protection from overturning of rigid block-like objects with linearquadratic regulator active control. *Struct. Control Health Monit.* **2020**, *27*, e2598. [CrossRef]
17. Fabrizio, C.; Di Egidio, A.; de Leo, A. Top disconnection versus base disco nnection in structures subjected to harmonic base excitation. *Eng. Struct.* **2017**, *152*, 660–670. [CrossRef]
18. Fabrizio, C.; de Leo, A.; Di Egidio, A. Tuned mass damper and base isolation: A unitary approach for the seismic protection of conventional frame structures. *J. Eng. Mech.* **2019**, *145*, 04019011. [CrossRef]
19. Wang, S.-J.; Hwang, J.S.; Chang, K.C.; Lin, M.H.; Lee, B.H. Analytical and experimental studies on midstory isolated buildings with modal coupling effect. *Earthq. Engng. Struct. Dyn* **2013**, *42*, 201–219. [CrossRef]
20. Pagliaro, S.; Di Egidio, A. Archetype dynamically equivalent 3-d.o.f. model to evaluate seismic performances of intermediate discontinuity in frame structures. *J. Eng. Mech.* **2022**, *148*, 04022004.
21. Marian, L.; Giaralis, A. Optimal design of a novel tuned mass-damper-inerter (TMDI) passive vibration control configuration for stochastically support-excited structural systems. *Probabilistic Eng. Mech.* **2014**, *38*, 156–164. [CrossRef]
22. Kuhnert, W.M.; Gonçalves, P.J.P.; Ledezma-Ramirez, D.F.; Brennan, M.J. Inerter-like devices used for vibration isolation: A historical perspective. *J. Frankl. Inst.* **2021**, *358*, 1070–1086. [CrossRef]
23. Wang, F.C.; Lee, C.H.; Zheng, R.Q. Benefits of the inerter in vibration suppression of a milling machine. *J. Frankl. Inst.* **2019**, *356*, 7689–7703. [CrossRef]
24. Ma, R.; Bi, K.; Hao, H. A novel rotational inertia damper for amplifying fluid resistance: Experiment and mechanical model. *Mech. Syst. Signal Process.* **2021**, *149*, 107313. [CrossRef]
25. Pietrosanti, D.; De Angelis, M.; Giaralis, A. Experimental seismic performance assessment and numerical modelling of nonlinear inerter vibration absorber (IVA)-equipped base isolated structures tested on shaking table. *Earthq. Eng. Struct. Dyn.* **2021**, *50*, 2732–2753. [CrossRef]
26. Brzeski, P.; Kapitaniak, T.; Perlikowski, P. Novel type of tuned mass damper with inerter which enables changes of inertance. *J. Sound Vib.* **2015**, *349*, 56–66. [CrossRef]
27. Pietrosanti, D.; De Angelis, M.; Basili, M. Optimal design and performance evaluation of systems with Tuned Mass Damper Inerter (TMDI). *Earthq. Eng. Struct. Dyn.* **2017**, *46*, 1367–1388. [CrossRef]
28. De Domenico, D.; Ricciardi, G. An enhanced base isolation system equipped with optimal tuned mass damper inerter (TMDI). *Earthq. Eng. Struct. Dyn.* **2018**, *47*, 1169–1192. [CrossRef]
29. De Domenico, D.; Impollonia, N.; Ricciardi, G. Soil-dependent optimum design of a new passive vibration control system combining seismic base isolation with tuned inerter damper. *Soil Dyn. Earthq. Eng.* **2018**, *105*, 37–53. [CrossRef]
30. Giaralis, A.; Taflanidis, A. Optimal tuned mass-damper-inerter (TMDI) design for seismically excited MDOF structures with model uncertainties based on reliability criteria. *Struct. Control. Health Monit.* **2018**, *25*, e2082. [CrossRef]
31. Pietrosanti, D.; De Angelis, M.; Basili, M. A generalized 2-DOF model for optimal design of MDOF structures controlled by Tuned Mass Damper Inerter (TMDI). *Int. J. Mech. Sci.* **2020**, *185*, 105849. [CrossRef]
32. De Domenico, D.; Deastra, P.; Ricciardi, G.; Sims, N.D.; Wagg, D.J. Novel fluid inerter based tuned mass dampers for optimised structural control of base-isolated buildings. *J. Frankl. Inst.* **2019**, *356*, 7626–7649. [CrossRef]
33. Javidialesaadi, A.; Wierschem, N.E. Design and performance evaluation of inerter-based tuned mass dampers for a ground acceleration excited structure. *Soil Dyn. Earthq. Eng.* **2021**, *140*, 106463. [CrossRef]
34. Di Egidio, A.; Contento, A. Improvement of the dynamic and seismic behaviour or rigid block-like structures with a hysteretic mass damper coupled with an inerter. *Appl. Sci.* **2022**, *127*, 11527. [CrossRef]
35. Wen, Y.K. Method for random vibration of hysteretic systems . *J. Eng. Mech.* **1976**, *102*, 249–263. [CrossRef]
36. Ma, F.; Zhang, H.; Bockstedte, A.; Foliente, G.; Paevere, P. Parameter Analysis of the Differential Model of Hysteresis. *J. Eng. Mech.* **2004**, *71*, 342–349. [CrossRef]
37. Constantinou, M.; Adnane, M. *Dynamics of Soil-Base-Isolated Structure Systems Report 4: Evaluation of Two Models for Yielding Systems*; Report to NSAF; Department of Civil Engineering, Drexel University: Philadelphia, PA, USA, 1987.
38. Makris, N.; Kampas, G. Seismic Protection of Structures with Supplemental Rotational Inertia. *J. Eng. Mech.* **2016**, *142*, 04016089. [CrossRef]
39. Thiers-Moggia, R.; Málaga-Chuquitaype, C. Seismic protection of rocking structures with inerters. *Earthq. Eng. Struct. Dyn.* **2018**, *48*, 528–547. [CrossRef]
40. Chopra, A.K. *Dynamics of Structures*; Prentice Hall, Inc.: Englewood Cliffs, NJ, USA, 1995.

41. Viola, E. *Fondamenti di Dinamica e Vibrazione Delle Strutture, 1st Volume*; Pitagora Editrice Bologna: Bologna, Italy, 2001.
42. Iervolino, I.; Galasso, C.; Cosenza, E. REXEL: Computer aided record selection for code-based seismic structural analysis. *Bull. Earthq. Eng.* **2010**, *8*, 339–362. [CrossRef]

Disclaimer/Publisher's Note: The statements, opinions and data contained in all publications are solely those of the individual author(s) and contributor(s) and not of MDPI and/or the editor(s). MDPI and/or the editor(s) disclaim responsibility for any injury to people or property resulting from any ideas, methods, instructions or products referred to in the content.